

APPLICATION OF THE IMPROVED FOUR-NODE ELEMENT MISQ24 FOR GEOMETRICALLY NONLINEAR ANALYSIS OF PLATE/SHELL STRUCTURES

Nguyen Van Hieu¹, Chau Dinh Thanh², Nguyen Huu Anh Tuan¹

¹Faculty of Civil Engineering, Ho Chi Minh City University of Architecture

²GACES, Faculty of Civil Engineering and Applied Mechanics,
Ho Chi Minh City University of Technical Education

(Received: 23/02/2014; Revised: 02/04/2014; Accepted: 16/06/2014)

ABSTRACT

In this paper the smoothed strain based four-node flat element MISQ24 with drilling degrees of freedom is extended for geometrically nonlinear analysis of plate and shell structures. The von-Karman's large deflection theory and the Total Lagrangian (TL) approach are employed in the formulation of the elements to describe small strain geometric nonlinearity with large deformations using the first-order shear deformation theory (FSDT). The predictive capability of the present models is demonstrated by comparing the present results with analytical/experimental and other numerical solutions available in the literature. Numerical examples show that the presented formulations can prevent loss of accuracy in severely distorted meshes, and therefore, are superior to those of other quadrilateral elements with in-planes rotations.

Keywords: Geometrically nonlinear analysis; plate/shell structures; smoothed finite element.

1. Introduction

The wide application of plate/shell structures in engineering practice has caught the interests of many researchers in the fields of developing simple and efficient plate/shell elements for geometrically nonlinear analysis of these structures. The accurate prediction of structural response characteristics in the large deformation regime therefore becomes more important considerations of engineering design.

Geometrically nonlinear analysis is usually performed iteratively for each load increment with subsequent updating of coordinates and internal stresses to obtain the equilibrium in the deformed configuration. As a result, geometrically nonlinear analysis is considered as a

complex issue that requires efficient and reliable advanced numerical methods. Numerical methods such as finite element methods have been developed and widely used for nonlinear analysis of these structures with complex geometry and loading history (Yang et al. (2000), Gal and Levy (2006)). Among different kinds of shell finite elements such as flat shell elements, curved shell elements and degenerated shell elements, the flat shell elements have been often and widely used owing to the ease to mix them with other types of element, the simplicity in their formulation and the effectiveness in performing computations (Yang et al. (2000), Gal and Levy (2006), Choi and Lee (2003), Pimpinelli (2004)).

The aim of this work is to further develop the flat element MISQ24, whose

performances in linear analysis have already been verified and demonstrated in references (Nguyen-Van et al. (2009, 2011)) for geometrically nonlinear analysis of composite plate and shell structures. The von-Karman's large deflection theory and the total Lagrangian (TL) approach are utilized in the small strain-large deformation formulation and then the solution of the nonlinear equilibrium equations is obtained by the arc-length method. With the aid of the assumed strain smoothing technique, the evaluations of the membrane, bending and geometric stiffness matrices are obtained via integration on the boundary of smoothing cells. This boundary integration contributes to the preservation of high accuracy of the method when highly distorted elements or coarse meshes are used. Numerical examples show that the present element is free from locking and exhibits good accuracy and stability in capturing geometric nonlinearity in plate/shell structures.

This paper is outlined as follows. A brief review of the FSDT finite element formulations for geometrically nonlinear analysis is first introduced. This is followed by the description of assumed strain smoothing approach for the generalized strain and the tangent stiffness matrix of the element are derived in Section 2. Some numerical examples are reported in Section 3 in order to verify and assess the performance of the proposed element. Finally, some concluding remarks are presented in Section 4.

2. Geometric nonlinear formulations of the MISQ24 element

2.1. The first-order shear deformation theory (FSDT) for nonlinear analysis

Based on the FSDT, the plate kinematics is governed by the midplane displacements u_0, v_0, w_0 and the rotations θ_x, θ_y of the normal to the mid-surface about y- and x-axis, respectively (Reddy (2004))

$$\begin{aligned} u(x, y, z) &= u_0(x, y) + z\theta_x, \\ v(x, y, z) &= v_0(x, y) + z\theta_y, \\ w(x, y, z) &= w_0(x, y). \end{aligned} \quad (1)$$

For large deformation analysis, the in-plane vector of Green-Lagrangian strain in a plate element is

$$\boldsymbol{\varepsilon} = \begin{Bmatrix} \varepsilon_x \\ \varepsilon_y \\ \varepsilon_{xy} \end{Bmatrix} = \begin{Bmatrix} u_{,x} + \frac{1}{2}(u_{,x}^2 + v_{,x}^2 + w_{,x}^2) \\ v_{,y} + \frac{1}{2}(u_{,y}^2 + v_{,y}^2 + w_{,y}^2) \\ u_{,y} + v_{,x} + (u_{,x}u_{,y} + v_{,x}v_{,y} + w_{,x}w_{,y}) \end{Bmatrix}, \quad (2)$$

Substituting Equation (1) into Equation (2) and considering the von Karman's large deflection assumption, the in-plane strain vector can be rewritten as

$$\boldsymbol{\varepsilon} = \boldsymbol{\varepsilon}_m + z\boldsymbol{\varepsilon}_b, \quad (3)$$

in which

$$\boldsymbol{\varepsilon}_m = \boldsymbol{\varepsilon}_m^L + \boldsymbol{\varepsilon}_m^{NL}, \quad \boldsymbol{\varepsilon}_m = \begin{Bmatrix} u_{0,x} + \frac{1}{2}w_{,x}^2 \\ v_{0,y} + \frac{1}{2}w_{,y}^2 \\ u_{0,y} + v_{0,x} + w_{,x}w_{,y} \end{Bmatrix} = \underbrace{\begin{Bmatrix} u_{0,x} \\ v_{0,y} \\ u_{0,y} + v_{0,x} \end{Bmatrix}}_{\text{linear part}} + \underbrace{\begin{Bmatrix} \frac{1}{2}w_{,x}^2 \\ \frac{1}{2}w_{,y}^2 \\ w_{,x}w_{,y} \end{Bmatrix}}_{\text{nonlinear part}} \quad (4)$$

$$\boldsymbol{\varepsilon}_b = \begin{Bmatrix} \theta_{,x,x} \\ \theta_{,y,y} \\ \theta_{,x,y} + \theta_{,y,x} \end{Bmatrix}. \quad (5)$$

The transverse shear strain vector is given as

$$\boldsymbol{\gamma} = \begin{Bmatrix} \gamma_{xz} \\ \gamma_{yz} \end{Bmatrix} = \begin{Bmatrix} \theta_x - w_{,x} \\ \theta_y - w_{,y} \end{Bmatrix}. \quad (6)$$

The constitutive relationship of the plate can be expressed as

$$\boldsymbol{\sigma}^* = \mathbf{D}^* \boldsymbol{\varepsilon}^*, \quad (7)$$

where

$$\boldsymbol{\sigma}^* = \begin{bmatrix} \mathbf{N} \\ \mathbf{M} \\ \mathbf{T} \end{bmatrix}, \quad \boldsymbol{\varepsilon}^* = \begin{bmatrix} \boldsymbol{\varepsilon}_m \\ \boldsymbol{\varepsilon}_m \\ \boldsymbol{\gamma} \end{bmatrix}, \quad \mathbf{D}^* = \begin{bmatrix} \mathbf{D}_m & \mathbf{0} & \mathbf{0} \\ \mathbf{0} & \mathbf{D}_b & \mathbf{0} \\ \mathbf{0} & \mathbf{0} & \mathbf{D}_s \end{bmatrix}, \quad (8)$$

and $\mathbf{N} = [N_x \ N_y \ N_{xy}]$ is the in-plane traction resultant, $\mathbf{T} = [Q_x \ Q_y]$ is the out-of-plane traction resultant and $\mathbf{M} = [M_x \ M_y \ M_{xy}]$ is the out-of-plane moment resultant. \mathbf{D}_m is the extensional stiffness, \mathbf{D}_b is the bending stiffness and \mathbf{D}_s is the transverse shear stiffness, which are given in detail in Reddy (2004).

geometric nonlinear analysis

As shown in Figure 1, a quadrilateral element domain Ω_c is further divided into nc smoothing cells. The generalized strain field is smoothed by a weighted average of the original generalized strains using the strain smoothing operation for each smoothing cell as follows.

2.2. Strain smoothing formulations for

$$\tilde{\boldsymbol{\varepsilon}}_m^L = \frac{1}{A_c} \int_{\Omega_c} \boldsymbol{\varepsilon}_m^L(\mathbf{x}) d\Omega \quad (9)$$

$$\tilde{\boldsymbol{\varepsilon}}_m^{NL} = \frac{1}{A_c} \int_{\Omega_c} \boldsymbol{\varepsilon}_m^{NL}(\mathbf{x}) d\Omega \quad (10)$$

$$\tilde{\boldsymbol{\varepsilon}}_b = \frac{1}{A_c} \int_{\Omega_c} \boldsymbol{\varepsilon}_b(\mathbf{x}) d\Omega \quad (11)$$

where $\tilde{\boldsymbol{\varepsilon}}_m^L$, $\tilde{\boldsymbol{\varepsilon}}_m^{NL}$, $\tilde{\boldsymbol{\varepsilon}}_b$ are the smoothed (averaged) strains and A_c is the area of the smoothing cell Ω_c .

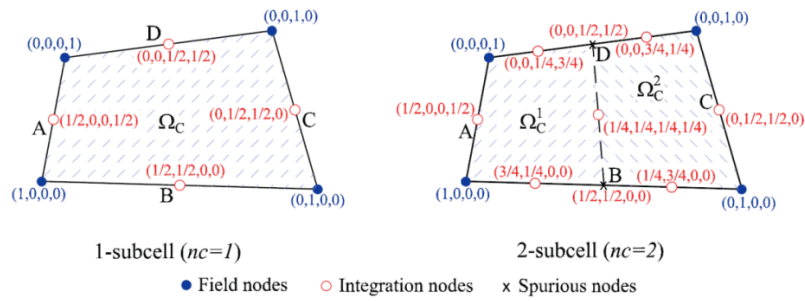


Figure 1. Subdivision of an element into nc smoothing cells and the values of shape functions at nodes in the format (N1,N2,N3,N4)

Introducing the approximation of the linear membrane strain by the quadrilateral finite element using Allman-type interpolation functions with drilling degrees of freedom (Ibrahimbegovic et al.

(1990)) and applying the divergence theorem, the smoothed membrane strain can be obtained as

$$\tilde{\boldsymbol{\epsilon}}_m^L = \frac{1}{A_c} \int_{\Gamma_c} \mathbf{n}(\mathbf{x}) \mathbf{u}(\mathbf{x}) d\Gamma = \frac{1}{A_c} \int_{\Gamma_c} \sum_{i=1}^4 \mathbf{n}(\mathbf{x}) N_i(\mathbf{x}) \mathbf{q}_i d\Gamma = \sum_{i=1}^4 \tilde{\mathbf{B}}_{mi}^L \mathbf{q}_i, \tag{12}$$

where

$$\tilde{\mathbf{B}}_{mi}(\mathbf{x}_C) = \frac{1}{A_c} \int_{\Gamma_c} \begin{pmatrix} N_i n_x & 0 & Nx_i n_x \\ 0 & N_i n_y & Ny_i n_y \\ N_i n_y & N_i n_x & Nx_i n_y + Ny_i n_x \end{pmatrix} d\Gamma \tag{13}$$

in which Nx_i , Ny_i are Allman's incompatible shape functions defined in Ibrahimbegovic et al. (1990) and n_x , n_y are the components of the outward unit vector \mathbf{n} normal to the boundary Γ_c .

Applying Gauss integration along 4 segments of the boundary Γ_c of the smoothing domain Ω_c , the above equation can be rewritten in algebraic form as

$$\tilde{\mathbf{B}}_{mi}(\mathbf{x}_C) = \frac{1}{A_c} \sum_{b=1}^4 \begin{pmatrix} \sum_{n=1}^{nG} w_n N_i(\mathbf{x}_{bn}) n_x & 0 & 0 \\ 0 & \sum_{n=1}^{nG} w_n N_i(\mathbf{x}_{bn}) n_y & 0 \\ \sum_{n=1}^{nG} w_n N_i(\mathbf{x}_{bn}) n_y & \sum_{n=1}^{nG} w_n N_i(\mathbf{x}_{bn}) n_x & 0 \end{pmatrix} + \frac{1}{A_c} \sum_{b=1}^4 \begin{pmatrix} 0 & 0 & \sum_{n=1}^{nG} w_n Nx_i(\mathbf{x}_{bn}) n_x \\ 0 & 0 & \sum_{n=1}^{nG} w_n Ny_i(\mathbf{x}_{bn}) n_y \\ 0 & 0 & \sum_{n=1}^{nG} w_n Nx_i(\mathbf{x}_{bn}) n_y + \sum_{n=1}^{nG} w_n Ny_i(\mathbf{x}_{bn}) n_x \end{pmatrix} \tag{14}$$

where nG is the number of Gauss integration points, \mathbf{x}_{bn} the Gauss point and w_n the corresponding weighting coefficients. The first term in Equation (14), which relates to the in-plane translations (approximated by bilinear shape functions), is evaluated by one

Gauss point ($nG=1$). The second term, associated with the in-plane rotations (approximated by quadratic shape functions), is computed using two Gauss points ($nG=2$).

In the similar way, the smoothed nonlinear membrane strain over the element domain Ω_c can be written as

$$\tilde{\boldsymbol{\varepsilon}}_m^{NL} = \sum_{i=1}^4 \tilde{\mathbf{B}}_{mi}^{NL} \mathbf{q}_i \tag{15}$$

where $\tilde{\mathbf{B}}_{mi}^{NL}$ is the smoothed nonlinear gradient matrix in the smoothing cell given as

$$\tilde{\mathbf{B}}_{mi}^{NL} = \tilde{\mathbf{H}} \tilde{\mathbf{G}}_i, \tag{16}$$

in which

$$\tilde{\mathbf{G}}_i = \frac{1}{A_c} \sum_{g=1}^4 \begin{pmatrix} 0 & 0 & N_i(\mathbf{x}_g^G) n_x & 0 & 0 \\ 0 & 0 & N_i(\mathbf{x}_g^G) n_y & 0 & 0 \end{pmatrix} l_g^c, \tag{17}$$

$$\tilde{\mathbf{H}} = \sum_{i=1}^4 \begin{pmatrix} \frac{1}{A_c} \sum_{j=1}^4 N_i(\mathbf{x}_j^G) n_x l_j^c w_i & 0 \\ 0 & \frac{1}{A_c} \sum_{j=1}^4 N_i(\mathbf{x}_j^G) n_y l_j^c w_i \\ \frac{1}{A_c} \sum_{j=1}^4 N_i(\mathbf{x}_j^G) n_y l_j^c w_i & \frac{1}{A_c} \sum_{j=1}^4 N_i(\mathbf{x}_j^G) n_x l_j^c w_i \end{pmatrix}, \tag{18}$$

and w_i is the deflection at the node i of the element.

The smoothed bending strain over the element domain Ω_c is expressed as

$$\tilde{\boldsymbol{\varepsilon}}_b = \sum_{i=1}^4 \tilde{\mathbf{B}}_{bi} \mathbf{q}_i, \tag{19}$$

where

$$\tilde{\mathbf{B}}_{bi} = \frac{1}{A_c} \sum_{b=1}^4 \begin{pmatrix} 0 & 0 & 0 & N_i(\mathbf{x}_b^G) n_x & 0 \\ 0 & 0 & 0 & 0 & N_i(\mathbf{x}_b^G) n_y \\ 0 & 0 & 0 & N_i(\mathbf{x}_b^G) n_y & N_i(\mathbf{x}_b^G) n_x \end{pmatrix} l_b, \tag{20}$$

The shear strain is expressed by independent interpolation fields in the natural coordinate systems as (Bathe and Dvorkin (1985))

$$\begin{bmatrix} \gamma_x \\ \gamma_y \end{bmatrix} = \mathbf{J}^{-1} \begin{bmatrix} \frac{1}{2}(1-\xi) & 0 & \frac{1}{2}(1+\xi) & 0 \\ 0 & \frac{1}{2}(1-\eta) & 0 & \frac{1}{2}(1+\eta) \end{bmatrix} \begin{bmatrix} \gamma_\eta^A \\ \gamma_\xi^B \\ \gamma_\eta^C \\ \gamma_\xi^D \end{bmatrix}, \tag{21}$$

where \mathbf{J} is the Jacobian matrix and the midside nodes A, B, C, D are shown in Figure 1.

Expressing $\gamma_\eta^A, \gamma_\eta^C$ and $\gamma_\xi^B, \gamma_\xi^D$ in terms of the discretized field \mathbf{q} , we obtain the shear gradient matrix

$$\bar{\mathbf{B}}_{si} = \mathbf{J}^{-1} \begin{bmatrix} N_{i,\xi} & b_i^{11} N_{i,\xi} & b_i^{12} N_{i,\xi} \\ N_{i,\eta} & b_i^{21} N_{i,\eta} & b_i^{22} N_{i,\eta} \end{bmatrix}, \tag{22}$$

where

$$b_i^{11} = \xi_i x_{,\xi}^M, \quad b_i^{12} = \xi_i y_{,\xi}^M, \quad b_i^{21} = \eta_i x_{,\eta}^L, \quad b_i^{22} = \eta_i y_{,\eta}^L \tag{23}$$

in which $\xi_i \in \{-1, 1, 1, -1\}$, $\eta_i \in \{-1, -1, 1, 1\}$, and $(i, M, L) \in \{(1, B, A); (2, B, C); (3, D, C); (4, D, A)\}$

Finally, the element tangent stiffness matrix $\tilde{\mathbf{K}}_T$ is modified as

$$\tilde{\mathbf{K}}_T = \tilde{\mathbf{K}}_L + \tilde{\mathbf{K}}_{NL} + \tilde{\mathbf{K}}_g, \tag{24}$$

where

$$\tilde{\mathbf{K}}_L = \sum_{i=1}^{nc} \tilde{\mathbf{B}}_{Li}^T \mathbf{D}^* \tilde{\mathbf{B}}_{Li} A_i + \gamma \int_{\Omega} \mathbf{b}^T \mathbf{b} d\Omega, \tag{25}$$

$$\tilde{\mathbf{K}}_{NL} = \sum_{i=1}^{nc} \tilde{\mathbf{B}}_{NLi}^T \mathbf{D}^* \tilde{\mathbf{B}}_{NLi} A_i, \tag{26}$$

$$\tilde{\mathbf{K}}_g = \sum_{i=1}^{nc} \tilde{\mathbf{G}}_i^T \hat{\mathbf{N}} \tilde{\mathbf{G}}_i A_i, \tag{27}$$

$$\tilde{\mathbf{B}}_L = \begin{bmatrix} \tilde{\mathbf{B}}_m^L \\ \tilde{\mathbf{B}}_b \\ \tilde{\mathbf{B}}_s \end{bmatrix}, \quad \tilde{\mathbf{B}}_{NL} = \begin{bmatrix} \tilde{\mathbf{B}}_m^{NL} \\ \mathbf{0} \\ \mathbf{0} \end{bmatrix}, \quad \hat{\mathbf{N}} = \begin{bmatrix} N_x & N_{xy} \\ N_{xy} & N_y \end{bmatrix}, \quad \mathbf{b}_i = \begin{bmatrix} -\frac{1}{2} N_{i,y} \\ -\frac{1}{2} N_{i,x} \\ -\frac{1}{2} (N_{x_{i,y}} + N_{y_{i,x}}) - N_i \end{bmatrix} \tag{28}$$

in which the positive penalty parameter $\gamma = G$ and the number of smoothing cells $nc = 2$ are chosen in this study.

The internal forces at the time t computed from the stress state in the structures can be rewritten as

$${}^t \tilde{\mathbf{F}} = \int_{\Omega} (\tilde{\mathbf{B}}_L + \tilde{\mathbf{B}}_{NL})^t \boldsymbol{\sigma}^* d\Omega, \tag{29}$$

in which the stress resultant after the i^{th} iteration is

$${}^t \boldsymbol{\sigma}_{i+1}^* = {}^t \boldsymbol{\sigma}_i^* + {}^t \Delta \boldsymbol{\sigma}^*, \tag{30}$$

Finally, the nonlinear equations can be rewritten as

$${}^t \tilde{\mathbf{K}}_T \Delta \mathbf{q} = {}^{t+\Delta t} \mathbf{P} - {}^t \mathbf{F} \tag{31}$$

3. Numerical results and Discussions

In this section, we will test and assess the MISQ24 element through numerical examples. In all examples, the arc-length

method and automatic incremental algorithm is used to solve the nonlinear finite element equations. The convergence tolerance of displacement is taken to be 0.001. Unless other specified, the shear correction factors are equal to 5/6, and SI units are used.

3.1. A clamped skew plate

The bending behaviour of a skew plate is often considered as a corner stress concentration problem due to a strong singularity in bending moments at the obtuse vertex. It is often avoided for nonlinear analyses of plate bending problems. Therefore, this section deals with the large deflection of clamped skew plates with different skew angles α from 0^0 to 60^0 as shown in Figure 2. The geometric

and material parameters are as follows: $a = 1.5b$; $h/a = 0.02$; $E = 2 \times 10^5$; $\nu = 0.3$; $D = Eh^3/(12(1-\nu))$. Two types of loading, namely a uniformly distributed load and a concentrated load are examined in this study. The full plate is modelled using 8×8 elements with regular as well as highly distorted shapes as shown in Figure 2.

The accuracy of the present solutions is investigated for both types of mesh with different skew angles $\alpha = 0^\circ, 30^\circ, 50^\circ, 60^\circ$. The load-deflection curves obtained by the present elements are plotted and compared with theoretical solutions of Chia (1980) and the hybrid mixed element's results of Duan and Mahendran (2003) as shown in Figure 3a-b.

It is followed from Figure 3a that the performance of the present elements are in good agreement with the theoretical solution for both types of mesh and the

present performance is better than those of the hybrid mixed element for the cases of skew angles $\alpha = 30^\circ$ and 60° when the plate is subjected to uniform load.

For the skew plates subjected to a point load, there is no analytical solution and the present results are compared very favorable with the solutions using hybrid mixed element of Duan and Mahendran (2003) for both types of mesh as can be seen in Figure 3b. Numerical results also show that the maximum central deflection decreases as the skew angle of the plate increases and the load-deflection curve of the plate with 60° skew angle approximates to a straight line. Therefore, the rigidity of skew plates can increase by increasing the skew angle and the overall strength of structures will improve.

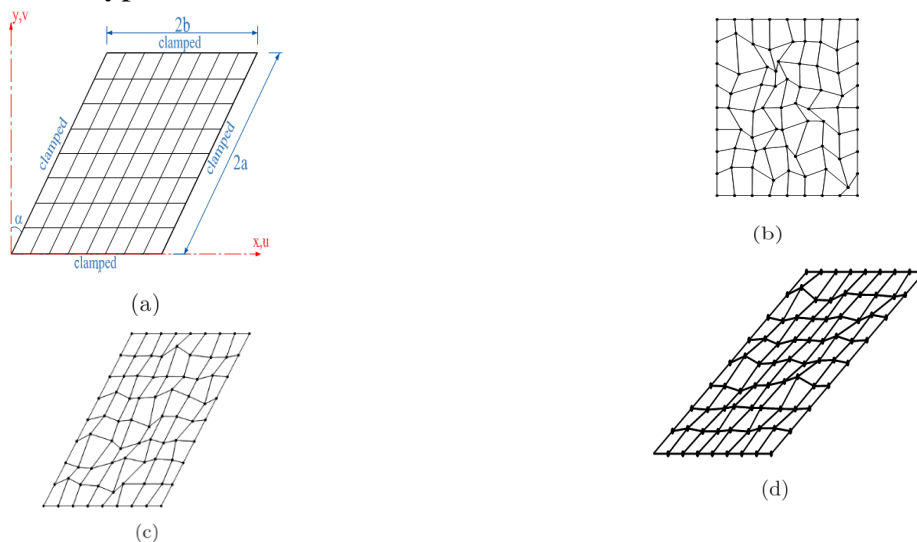


Figure 2. Meshes of a clamped skew plate: (a) 8×8 regular mesh; (b) 8×8 irregular mesh with $\alpha = 0^\circ$; (c) 8×8 irregular mesh with $\alpha = 30^\circ$; (d) 8×8 irregular mesh with $\alpha = 60^\circ$

The effect of span-to-thickness (a/h) ratios on the nonlinear bending behaviour of the above clamped skew plate is also studied for three values, namely $a/h = 10, 100, 1000$ using a distorted mesh of 8×8

MISQ24 elements. Figure 4a illustrates the load-deflection curves for the case of the uniformly distributed load while the load-deflection curves for the concentrated load are displayed in Figure 4b. It is found that

the effect of the span-to-thickness ratio on the central deflections has no influence for thin skew plates with $a/h > 100$ in both cases of loading. For the plates under the distributed load, the effect of the span-to-thickness ratio has a minor effect on the deflection when skew angle $\alpha < 30^\circ$ while

it have a greater effect for any skew angle α from 0° to 60° in the case of the point load. It is also observed that the degree of nonlinearity in the thick 60° skew plate is more pronounced than in the thin plate owing to the dominance of transverse shear deformation for both cases of loading.

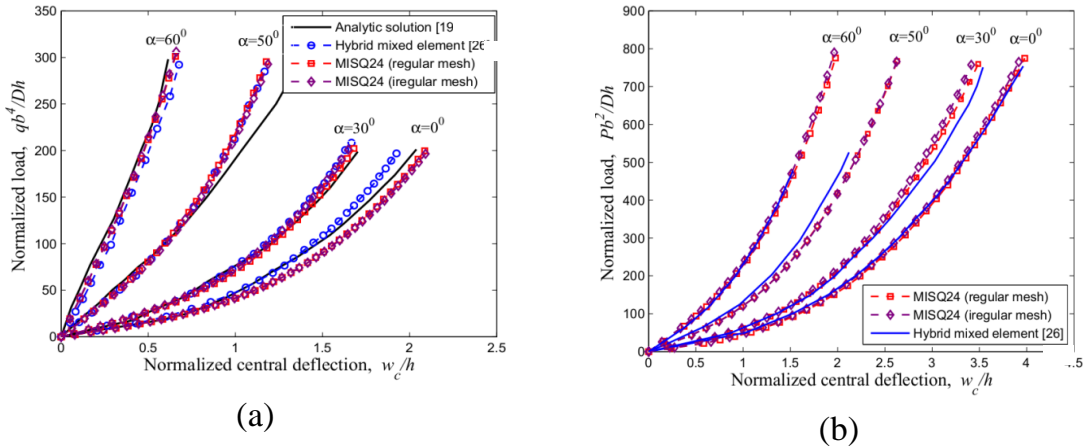


Figure 3. Load-deflection responses of the clamped skew plate: (a) under a uniform load and (b) under a point load

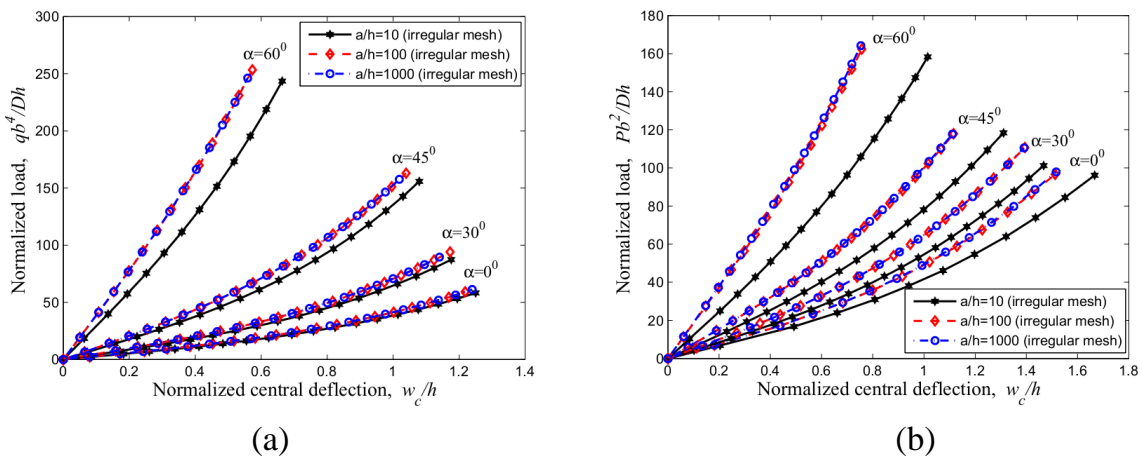


Figure 4. Effect of span-to-thickness ratios to load-deflection responses of the clamped skew plate: (a) under a uniform load and (b) under a point load

3.2. A hinged cylindrical shell under point load

This section is concerned with the effect of thickness-to-length ratios effect on the nonlinear bending behaviour of a cylindrical shell subjected to a concentrated central load as shown in the

Figure 5. Two longitudinal edges of the shell are hinged, whereas the curved edges are free. The length of the shell panel is $L = 508$ mm with a shell radius $R = 2540$ mm and an open angle $2\phi = 0.2$ rad. The material properties are: $E = 3.10275$ kN/mm², $\nu = 0.3$. Two different thickness, namely $h = 12.7$ mm and $h = 6.35$ mm are

examined in this study. Owing to symmetry, only a quadrant of shell is analysed with a 6×6 uniform mesh and distorted mesh as shown in Figure 5.

Figure 6a illustrates the nonlinear bending response of the shell panel with the thickness $h = 12.7$ mm. The nonlinear

solutions given by Sabir and Lock (1973), Crisfield (1979) and Sze et al. (2004) are also plotted in this figure for comparison. A snap-through behaviour is observed for this shell panel. It can be seen that five curves agree well together with the same limit points.

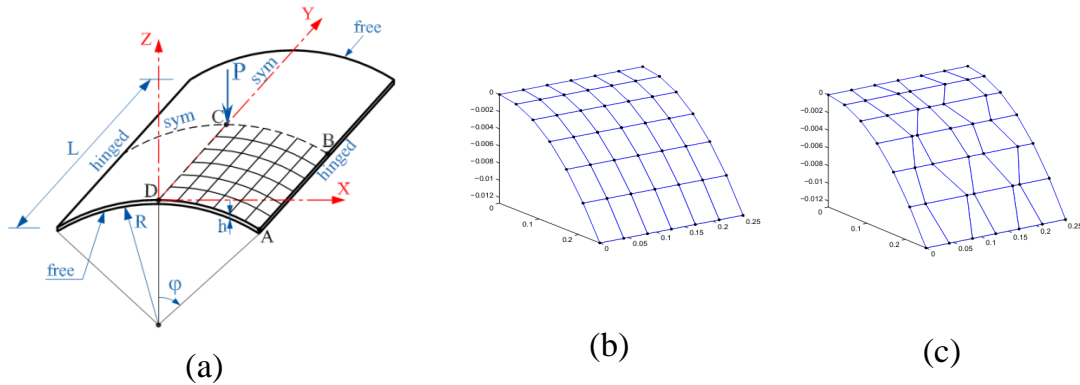


Figure 5. A hinged cylindrical shell: (a) geometry and boudary conditions; (b) 6×6 regular mesh and (c) 6×6 irregular mesh

Figure 6b shows the load-deflection relationship curves for the shell panel with the thickness $h = 6.35$ mm. A snap-back phenomenon is noticed for this shell panel. The present solutions for both types of mesh are compared with the results computed by Sze et al. (2004). It is clearly investigated that the present method has

successfully captured the negative load limit point and the present results agree well with those given in literature with only small disparities. These differences may be due to the coarse mesh and the solution strategies.

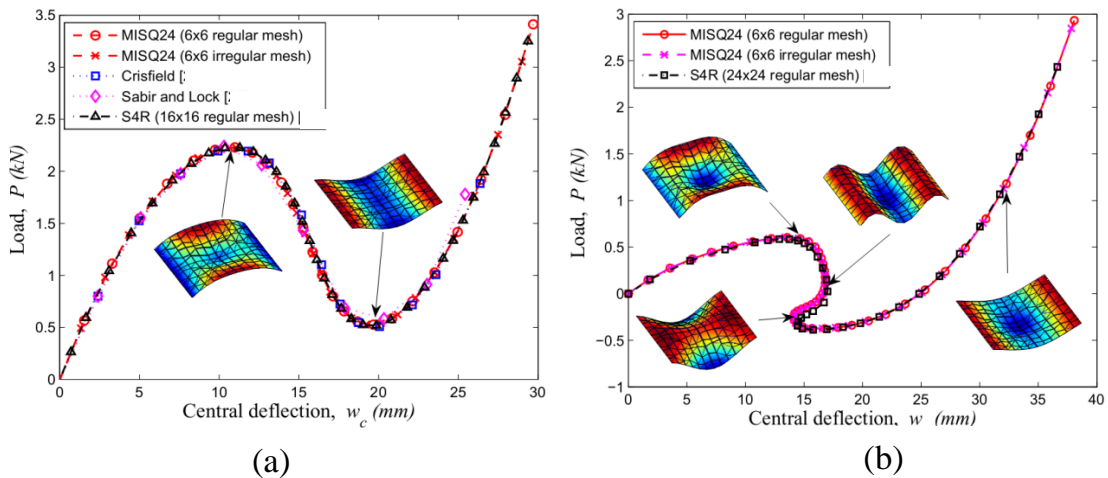


Figure 6. Load-deflection responses of the hinged cylindrical shell: (a) $h = 12.7$ mm; (b) $h = 6.35$ mm

4. Conclusion

In this paper, the MISQ24 element is further developed and successfully applied to geometrically nonlinear analysis of plate and shell structures in the framework of the FSDT. Numerical examples have been carried out and the present element is found to yield satisfactory results in comparison with other available finite element solutions as well as experimental

results. It is observed that the present approach remains accurate even with coarse meshes or badly-shaped elements. In addition, the present element has the advantage of being simple in formulation and ready for use in analysis of both plate and shell structures with a minimal amount of effort to implement. The success of the present flat/shell element provides a further demonstration of efficient flat quadrilateral elements for nonlinear analysis.

REFERENCES

- Bathe K. J., Dvorkin E. N 1985, 'A four node plate bending element based on Mindlin-Reissner plate theory and a mixed interpolation', *International Journal for Numerical Methods in Engineering*, Vol. 21, pp. 367–383.
- Chia C. Y 1980, *Nonlinear Analysis of Plate*, McGraw-Hill: New York.
- Choi C. K, T., Lee Y 2003, 'Efficient remedy for membrane locking of 4-node flat shell elements by non-conforming modes', *Computer Methods in Applied Mechanics and Engineering*, Vol. 192, pp. 1961–1971.
- Crisfield M. A 1979, 'A fast modified Newton-Raphson iteration', *Computer Methods in Applied Mechanics and Engineering*, Vol. 20, pp. 267–278.
- Duan M., Mahendran M 2003, 'Large deflection analyses of skew plates using hybrid/mixed finite element method', *Computers and Structures*, Vol. 81, pp. 1415–1424.
- Gal E., Levy R 2006, 'Geometrically nonlinear analysis of shell structures using a flat triangular shell finite element', *Archives of Computational Methods in Engineering*, Vol. 13, pp. 331–388.
- Ibrahimbegovic A., Taylor R. L., Wilson E. L 1990, 'A robust quadrilateral membrane finite element with drilling degrees of freedom', *International Journal for Numerical Methods in Engineering*, Vol. 30, pp. 445–57.
- Nguyen-Van H., Mai-Duy N., Tran-Cong T 2009, 'An improved quadrilateral flat element with drilling degrees of freedom for shell structural analysis', *CMES: Computer Modeling in Engineering & Sciences*, Vol. 49 (2), pp. 81-112.
- Nguyen-Van H., Mai-Duy N., W. Karunasena, Tran-Cong T 2011, 'Buckling and vibration analysis of laminated composite plate/shell structures via a smoothed

- quadrilateral flat shell element with in-plane rotations’, *Computers and Structures*, Vol. 89, pp.612-625.
- Pimpinelli G 2004, ‘An assumed strain quadrilateral element with drilling degrees of freedom’, *Finite Element in Analysis and Design*, Vol. 41, pp. 267–283.
- Reddy, J.N 2004, *An Introduction to Nonlinear Finite Element Analysis*, Oxford university press.
- Sabir A. B., Lock A. C 1973, ‘The application of finite elements to large deflection geometrically nonlinear behaviour of cylindrical shells’, in: *C. A. Brebbia, H. Tottenham (Eds.), Variational Methods in Engineering*, Southampton Univeristy Press
- Sze K. Y., Liu X. H., Lomboy S. H. 2004, ‘Popular benchmark problems for geometric nonlinear analysis of shells’, *Finite Element in Analysis and Design*, Vol. 40, pp. 1551–1569.
- Yang H. T. Y., Saigal S., Masud A., Kapania R. K 2000, ‘A survey of recent shell element’, *International Journal for Numerical Methods in Engineering* Vol. 47 (1-3), pp. 101–127.